Sex- and Age-Specific Development of ssRNA Virus Receptor Expression in the Human Brain

Leanne Monteiro[1*] Negeen Halabian[1*] Jiawei Li[2] Maheshwar Panday[1] Nadine Barone[1] Kathryn M. Murphy[1,2]

[1] McMaster Neuroscience Graduate Program, McMaster University, Hamilton, ON, L8S 4K1, Canada
[2] Department of Psychology, Neuroscience & Behavior, McMaster University, Hamilton, ON, L8S 4K1, Canada
* These authors contributed equally to this work and share first authorship

Correspondence should be addressed to Kathryn M. Murphy; kmurphy@mcmaster.ca
Kathryn Murphy, Department of Psychology, Neuroscience & Behavior, McMaster University, McMaster University, 1280 Main Street West, Hamilton, ON L8S 4K1, Canada.

Keywords: Human, Brain, Development, Virus receptors, Sex-specific differences, Gene expression, Lifespan, High-dimensional analyses

Abstract

The COVID-19 pandemic highlighted the detrimental impact of neuroinvasive single-stranded RNA (ssRNA) viruses. Those viruses cause a wide range of human diseases ranging from mild to severe life-threatening conditions. Host factors, including age, sex, and virus receptor expression, influence infection severity; yet, how sex and age shape the expression of ssRNA virus receptors in the human brain remains unclear. Here, we applied a data-driven computational workflow that integrates sex and age to characterize developmental patterns of ssRNA virus receptors in females and males across the human brain. Using a publicly available transcriptomic dataset spanning the lifespan, we analyzed 67 host receptor genes that mediate viral entry across 10 families of ssRNA viruses. Lifespan trajectories were generated, and high-dimensional analyses compared changes between sexes across 15 brain areas (n = 700, F = 306, M = 394; age range: 4 months–82 years), revealing spatiotemporal patterns of virus receptor expression. Unsupervised hierarchical clustering of the 2010 trajectories identified 25 different patterns spanning a range of sex bias from female-biased to male-biased expression. Differential expression analysis revealed a brain-wide pattern of sex differences in virus receptor expression during childhood, prior to puberty. Among virus families, *Pneumoviridae* was the most sexually dimorphic, and cortical brain areas had distinct developmental trajectories for females and males. While females are often described as developing precociously relative to males, our findings show that sex differences in virus receptor expression are not simple linear shifts, but follow complex high-dimensional trajectories, underscoring the importance of incorporating sex as a biological variable in studies of neuroinfectious disease vulnerability.

Introduction

The COVID-19 pandemic, Zika virus outbreak, and rising Dengue fever cases highlight the escalating public health threat of neuroinfectious diseases caused by single-stranded RNA (ssRNA) viruses (Bohmwald et al., 2018; Morgello, 2020; Sun et al., 2020). Climate change is accelerating this threat by expanding the range of mosquito- and tick-borne viruses into new regions, increasing global exposure and transmission. These viruses can reach the brain through direct or indirect routes and trigger neurological symptoms ranging from headache, anosmia, and confusion to encephalitis, stroke, and death (Koyuncu et al., 2013; Engin et al., 2021; Nath and Johnson, 2022).

The intensity, persistence, and fatality of these outcomes vary widely among individuals and are strongly influenced by host factors such as sex and age (Mauvais-Jarvis et al., 2020; Zhou et al., 2020; Jacobsen and Klein, 2021; Sudre et al., 2021). For example, men and older adults are more likely to experience severe COVID-19, SARS, and MERS (Jacobsen and Klein, 2021; Kumar et al., 2021), whereas women show higher morbidity and mortality from influenza and greater persistence of post-acute sequelae such as Long COVID (Klein and Huber, 2009; Scully et al., 2020; Sudre et al., 2021). These differences highlight the importance of host biology in shaping vulnerability to infection.

Despite this, little is known about how virus receptor expression in the human brain varies by sex and age. Receptors such as hACE2, TMPRSS2, and NRP1 mediate viral entry, yet their developmental regulation in cortical and subcortical structures remains poorly characterized. This gap is significant given recent evidence that SARS-CoV-2 can induce neuron–glia fusion via these receptors (Martínez-Mármol et al., 2023) and that severe infections can leave behind

structural and transcriptomic signatures resembling brain aging (Douaud et al., 2022; Mavrikaki et al., 2022).

Here, we use transcriptomic data to map lifespan trajectories of ssRNA virus receptor expression in the human brain. Our data-driven computational workflow integrates sex as a biological variable, enabling the identification of robust sex- and age-related differences. Across cortical and subcortical regions, we observed distinct developmental patterns, with the greatest sex differences occurring during childhood, which may underlie population differences in neurological outcomes following viral infection.

Methods

Human transcriptomic dataset

The Hamilton Integrated Research Ethics Board approved this study. We analyzed postnatal human brain transcriptomic data from Kang et al., 2011 (GSE25219). This publicly available dataset spans a wide age range, providing the most comprehensive view of lifespan changes in the human brain. It includes exon-level transcriptome data from multiple brain areas, representing both sexes and diverse ethnicities. Brain samples were obtained from multiple repositories, including Yale University School of Medicine, NIMH Clinical Brain Disorders Branch, and the Human Fetal Tissue Repository at AECOM. The original study implemented rigorous quality checks (PMI, pH, RIN, DS), and none of these factors were significantly correlated with expression levels. A detailed description of tissue acquisition, processing, quality control, and validation can be found in the Supplementary Material from Kang et al. (2011).

We analyzed postnatal samples from 15 brain areas (n = 700; 306 females, 394 males) spanning ages 4 months to 82 years. We focused on areas with sufficient sampling across both sexes, including 11 cortical (OFC, DFC, VFC, MFC, M1C, S1C, IPC, A1C, STC, ITC, V1C) and 4 subcortical areas (HIP, AMY, MD, CBC). Detailed sample information and causes of death are provided in Supplementary Table 1. In this study, ‘sex’ refers to the biological and molecular characteristics of the tissue samples, as donor gender was not recorded. Notably, none of the cases used in the current study died from a viral disease.

Data preparation

We retrieved the processed and normalized data from Gene Expression Omnibus (GSE25219) and reformatted it into a working file for this study (Monteiro et al., 2025). This file included 17,528 protein-coding genes with associated metadata (age, sex, brain area, PMI, cause of death, etc.). From the 28 brain areas in the original dataset, 13 were excluded due to insufficient sample size for lifespan trajectory analysis, leaving 15 areas for downstream analyses.

Virus receptors

We examined 67 host receptor genes that mediate entry of ssRNA viruses into human cells, including known SARS-CoV-2 factors. Receptor genes were identified using a curated virus receptor database (http://computationalbiology.cn:5000/viralReceptor/type?type=4) (Zhang et al., 2019). These 67 receptors represent 10 viral families: *Arenaviridae*, *Coronaviridae, Filoviridae, Flaviviridae, Orthomyxoviridae, Paramyxoviridae, Picornaviridae, Pneumoviridae, Rhabdoviridae, and Togaviridae* (see Supplementary Table 2).

Visualization of lifespan trajectories

For each virus receptor gene in a brain area, expression values were z-scored to emphasize lifespan-related changes rather than absolute levels. Lifespan trajectories were then fitted separately for females and males using LOESS smoothing (span = 0.75, 128 points, 95% CI). LOESS was chosen because it captures both linear and nonlinear trends without imposing a predefined model. Age was plotted on a $\log_2$ scale to highlight rapid developmental changes in early life versus slower changes in adulthood. In total, 2010 trajectories were generated (67 receptor genes × 15 brain areas × 2 sexes) (Supplementary Fig. 1).

Clustering of trajectories

We applied hierarchical clustering (ward.D2 method) to group trajectories with similar lifespan patterns. Clustering was performed at two levels: (1) all trajectories and (2) trajectories grouped by virus family. The optimal number of clusters (k) was selected using the elbow method. For each cluster, an average trajectory was generated to capture its representative developmental pattern. Finally, we validated the uniqueness of the cluster trajectories using the Fréchet distance metric to compare the shapes of the trajectories while maintaining the orderly progression of age (Alt and Godau, 1995). The Fréchet distance is 0 for identical trajectories, and increases as the difference between trajectories becomes larger. All pairwise comparisons between the cluster trajectories were made, and the resulting Fréchet distances were analyzed using Estimation statistics (Calin-Jageman and Cumming, 2019; Ho et al., 2019). In all cases, within-cluster distances were smaller than between-cluster distances, validating the unique patterns of molecular brain development identified by the trajectory clusters (Supplementary Fig. 2).

Quantifying sex differences

Clusters were labeled based on the ratio of female to male trajectories. For example, a cluster labeled F100:M0 contained only female trajectories. Two complementary measures of sex bias were then computed:

Sex Bias Index (SBI): The SBI was calculated for each cluster to quantify the relative representation of female versus male trajectories. SBI values range from +1 (female-only) to -1 (male-only), computed as:

Equation 1: $$SBI = \frac{(number\ of\ Female\ Trajectories - number\ of\ Male\ Trajectories)}{(number\ of\ Female\ Trajectories + number\ of\ Male\ Trajectories)}$$

Dimorphism Score (DS): The DS was calculated as a global measure of sex bias for each virus family, defined as the average absolute SBI across clusters. DS values range from 0, indicating equal representation of female and male trajectories, to +1, indicating complete segregation by sex:

Equation 2: $$DS = \frac{|SBI\ cluster\ 1| + |SBI\ cluster\ 2| + \ldots}{(number\ of\ clusters)}$$

Differential expression-sliding window analysis (DE-SWAN)

To identify virus receptor genes with different expression levels between females and males across the lifespan, we applied Differential Expression-Sliding Window Analysis (DE-SWAN) (Lehallier et al., 2019). Differential expression was tested at each point along the LOESS-fitted trajectory using a fixed-size window centered on that point. To evaluate robustness, we tested window sizes of ±4, ±10, and ±20 LOESS points and assessed consistency across multiple significance thresholds ($p = 0.001$, 0.01, and 0.05). P-values were corrected for false discovery using the Benjamini-Hochberg procedure, generating q-values (Supplementary Fig. 3). At each window center, the number of significantly differentially expressed genes ($q < 0.05$) was counted and plotted as a function of age. Inflection points from the plot (peaks and troughs) were used to define age windows for downstream analysis. Window centers were determined from LOESS trajectories pooled across all genes, brain area, and sex. These centers were then consistently applied to generate DE-SWAN heatmaps for each individual brain area. Twelve windows were identified, centered at the following reference ages: 1, 1.5, 2, 3, 5, 8, 12, 16, 24, 32, 45, and 60 years. Differential expression was visualized as heatmaps, with rows representing genes, columns representing reference ages, and colours indicating directionality of expression between the sexes (magenta = female > male, green = male > female).

Visualizing high-dimensional developmental trajectories across 15 brain areas

To characterize sex-specific developmental patterns across all brain areas, we visualized the high-dimensional trajectories of 67 virus receptor genes separately for females and males. We applied a density-preserving modification of t-distributed stochastic neighbor embedding (den-SNE), implemented via the densvis package (Narayan et al., 2021), to project the high-dimensional data into a two-dimensional (2D) space while preserving both local and global structure in the data. For this analysis, the data were organized at the brain area level. A matrix was created with 30 rows (15 brain areas × 2 sexes) and 8,576 columns corresponding to 128 LOESS-fitted values for each of the 67 genes. Hierarchical clustering was applied to these brain area–sex trajectories to identify groups with similar developmental patterns. The resulting 2D den-SNE plots were then colour-coded based on cluster assignment derived from unsupervised hierarchical clustering of brain area–sex trajectories or metadata (e.g., sex or age).

Results

Non-linear, undulating development of virus receptors in female and male brains

We used a data-driven approach to map the development of virus receptors across the human lifespan and to assess sex differences (Fig. 1). Rather than age-binning the data, we fit LOESS curves separately to female and male samples, producing continuous trajectories that capture gradual changes in expression across development. This generated 2010 trajectories (67 receptor genes × 15 brain areas × 2 sexes) with each trajectory representing the expression of a single virus receptor gene in a specific brain area and sex.

An example is shown for SARS-CoV-2 receptor ACE2 (angiotensin-converting enzyme 2) (Fig. 2), where trajectories illustrate the non-linear, undulating changes that are common across virus receptor genes (Supplementary Fig. 1). In many cases, female and male trajectories followed different patterns, sometimes moving in opposite directions at the same ages (e.g., ACE2 in VFC, OFC, STC).

Unsupervised clustering of all 2010 trajectories, independent of sex, identified 25 distinct developmental patterns (Fig. 3A). Cluster composition (gene, brain area, sex) is listed in Supplementary Table 3. To assess the similarity of the cluster trajectories, we applied Fréchet distance analysis (Alt and Godau, 1995) and estimation statistics (Calin-Jageman and Cumming, 2019; Ho et al., 2019), which confirmed strong differences between clusters, validating them as distinct developmental cluster trajectories (Supplementary Fig. 2).

Each cluster was annotated using the ratio of female to male trajectories (Fig. 3B). The cluster trajectories exhibited a range of sex biases and developmental patterns that included

monotonic increases or decreases (e.g., clusters F30:M70 and F36:M64(1), respectively). However, most trajectories displayed non-linear undulating waves of gene expression with peaks and troughs occurring at different ages across the lifespan (e.g., F100:M0, F13:M87)(Fig. 3B). Some clusters were strongly biased toward females (e.g., F100:M0, F97:M3) or males (e.g., F13:M87, F4:M96), while others contained both sexes in roughly equal proportions (e.g., F47:M53).

To quantify sex bias in each trajectory, we calculated a Sex Bias Index (SBI) for each cluster. Clusters spanned a wide range of sex biases, with SBI values ranging from +1 (female-only) to –0.91 (male-dominated). Overall, 8 clusters were female-biased (SBI range 1.00 to 0.26), 6 had a roughly equal number of male and female trajectories (SBI range 0.17 to -0.24), and 11 had more male than female trajectories (SBI range -0.26 to -0.91) (Fig. 4A).

Comparisons of strongly biased clusters revealed distinct developmental peaks. For example, male-biased trajectories (F13:M87) peaked around 2 years. In contrast, the comparable female-biased cluster (F100:M0) peaked slightly later at ~3 years (Fig. 4B). In addition, the two other strongly sex-biased clusters had trajectories that were opposite; the female-biased trajectory (F97:M3) declined through childhood, while the male-biased trajectory (F4:M96) increased (Fig. 4B). Across all 2010 trajectories, most local maxima occurred in early childhood (0–4 years), with a secondary peak in older adults (60–70 years) (Fig. 4C).

Cluster composition analyses revealed minimal overlap between sexes (Fig. 5). Nine clusters contained no overlapping female and male trajectories, despite broadly representing all 15 brain areas (Fig. 6) and all 10 virus families (Fig. 7). Exceptions were two male-biased clusters (F13:M87, F4:M96), which were dominated by a smaller set of areas (mainly A1C and MD).

Together, these analyses reveal that the complex spatiotemporal development of ssRNA virus receptors in the human brain is characterized by non-linear, undulating trajectories and widespread sex differences across brain areas and virus families.

A range of sexual dimorphism among the virus families

We next examined sex differences in virus receptor trajectories across the 10 ssRNA virus families (Supplementary Fig. 4). For each virus family, we applied the same unsupervised clustering approach. Each family had a range of different gene-brain area trajectories, some with monotonic increases or decreases, but most clusters had undulating trajectories of gene expression across the lifespan (Supplementary Fig. 4).

Inspection of the SBI for the clusters in each virus family identified a spectrum of sex biases, from female-only to male-only (Fig. 8A-J). Noting that some virus families had more sex-biased clusters than others, we calculated a Dimorphism Score (DS) for each family and plotted the distribution (Fig. 8K). The DS represented the overall sex bias for each family and had a value of 1 if all clusters had data from only one sex and 0 if there was an equal representation of female and male trajectories across all clusters. All families showed some degree of dimorphism, though the magnitude varied.

The *Pneumoviridae* family exhibited the strongest sex differences (DS = 0.67), with nearly all clusters biased toward either females or males and minimal overlap between trajectories. *Paramyxoviridae* (DS = 0.60) and *Coronaviridae* (DS = 0.51) also showed pronounced sex-biased trajectories. *Togaviridae, Picornaviridae*, *Rhabdoviridae,* and *Filoviridae* showed intermediate dimorphism (DS = 0.42–0.53), typically with both female- and male-biased

clusters. By contrast, *Flaviviridae* (DS = 0.30) and *Arenaviridae* (DS = 0.33) showed the weakest sex differences, with most clusters balanced between sexes.

Overall, sexual dimorphism in receptor expression is widespread but not uniform across viral families. The strongest differences were observed for *Pneumoviridae*, *Paramyxoviridae*, and *Coronaviridae*, highlighting families with potential sex-specific vulnerability to neuroinfectious disease.

Differential gene analysis identified a brain-wide pattern of early sex differences

To examine sex- and age-specific differences in expression of the 67 virus receptor genes across the 15 brain areas, we applied the DE-SWAN sliding window approach (Lehallier et al., 2019). This method compared female and male expression profiles across 12 overlapping age windows spanning the lifespan. Results were visualized as heatmaps (Fig. 9), with hierarchical clustering grouping genes that shared similar differential expression patterns across sex and age. The heatmaps highlighted genes exhibiting higher expression in females (magenta) or males (green) at specific ages, revealing clusters of receptors with shared patterns of sex-biased expression throughout development.

Across brain areas, sex differences were most frequent in childhood (0–12 years), with fewer differences in adulthood. In older adults, variation among brain areas increased: for example, nearly half of the genes in DFC showed sex differences, while V1C showed relatively few (Fig. 9 B & K). Thus, the DE-SWAN analysis identified a brain-wide pattern where the majority of sex differences in virus receptor gene expression occurred before puberty, with more heterogeneous patterns emerging later in life.

Sex-specific virus receptor development in the cortex

To determine whether virus receptor developmental programs were driven primarily by brain area or sex, we applied hierarchical clustering to the brain area–sex trajectories and visualized the high-dimensional relationships using density-preserving tSNE (den-SNE) (Narayan et al., 2021), which preserves both local and global structure. Hierarchical clustering identified four distinct clusters, which were colour-coded on the den-SNE plot (Fig. 10A). Two large clusters contained most brain areas but were predominantly sex-specific: one cluster included male-only trajectories, and the other contained mostly female trajectories, with the exception of male HIP. The two smaller clusters contained trajectories from both sexes and included CBC or MD data.

These results indicate that sex, rather than brain area, is the main driver of diversity in virus receptor trajectories across most areas. Colouring the den-SNE plot by age revealed no consistent age-related pattern (Fig. 10B). In contrast, colouring by sex and cortical versus subcortical identity revealed a striking sex-specific separation: the 11 cortical areas were clearly divided by sex, whereas trajectories for the four subcortical areas (AMY, HIP, MD, CBC) showed minimal divergence (Fig. 10C).

This spatial separation of female and male cortical areas supports the conclusion that virus receptor development in the human cortex follows distinct sex-specific programs. Importantly, these programs do not represent simple temporal shifts in development between sexes; rather, they reflect fundamentally unique developmental trajectories for females and males.

Discussion

This study characterized the sex-specific development of 67 ssRNA virus receptor genes in the human brain. High-dimensional analyses of lifespan trajectories revealed that most genes showed non-linear, undulating changes across development. Surprisingly, many genes followed sex-specific trajectories. Every virus family examined showed some degree of sexual dimorphism, with the strongest differences in the *Pneumoviridae* virus family. Sliding window analyses (DE-SWAN) revealed that most sex differences occurred during childhood, before puberty. Notably, compared with subcortical areas, cortical areas displayed a pronounced sex divergence, with females and males following distinct high-dimensional trajectories.

The gene-, age-, and sex-specific patterns we identified in this study may help explain differences in neurological symptoms caused by viral infections. For example, the stronger immune response often observed in females has been thought to underlie their better outcomes (Scully et al., 2020; Takahashi et al., 2020). Our findings suggest that receptor expression itself may also play a role, contributing to variation in severity, comorbidity, and symptom presentation. This interpretation is consistent with observational data showing that sex differences in outcomes are both age- and virus-specific (Peretz et al., 2015), and that the presence or absence of particular host factors can influence infection risk (Song et al., 2021; Martínez-Mármol et al., 2023). Our work identifies virus receptor expression as an additional host factor that may shape susceptibility and variability in neurological outcomes. Future studies will be needed to determine the functional consequences of these sex- and age-related differences, and to explore additional viral entry factors such as clathrin, adhesion molecules, and glycosaminoglycans, which may also show sex-specific expression. Those insights could

inform prevention and management strategies, even for asymptomatic individuals who may still experience long-term neurological effects.

Limitations

We designed this study specifically to assess sex- and age-related differences in virus receptor expression in the human brain. To do so, we adopted a sensitive bioinformatics framework for detecting non-linear developmental changes (Lehallier et al., 2019, 2020). LOESS regression was used to fit trajectories because it adapts flexibly to local patterns without forcing cases into arbitrary age bins or imposing predefined models. Unsupervised clustering then grouped trajectories objectively, without *a priori* knowledge about sex, gene, or brain area. As with all studies using the rare and valuable resources of developmental postmortem brain tissue, this study had a limited number of cases to analyze. To help mitigate this limitation, we used the most extensive developmental transcriptomic dataset available (Kang et al., 2011) and applied high-dimensional, data-driven methods that take advantage of all the data in a way that borrows power across all the samples. These approaches allowed us to detect subtle, non-linear, sex-specific developmental programs that would not be visible with traditional methods.

It is also important to recognize that factors beyond biology, such as gender, socioeconomic status, and healthcare access, contribute to differences in the neurological impact of viral infection. However, such information is not collected by brain banks. In addition, our study used transcriptomic data from donors whose causes of death include accidents and a range of non-viral diseases, making it difficult to disentangle how different causes of death may have influenced virus receptor gene expression in the brain. The design of this study, which combines a comprehensive lifespan dataset with sensitive trajectory analyses, enabled us to uncover new

insights into sex differences in virus receptor development in the human brain. Nevertheless, larger datasets will be needed to fully understand the impact of host factors on vulnerability to neuroinvasive viral infection.

Sex differences within virus families and brain areas

The diversity of trajectories and the minimal overlap between females and males highlight the complex molecular environment for viral infections in the brain. Every virus family contained at least one trajectory pattern that was strongly sex-biased, and most had at least one cluster dominated by either females or males. While many of these patterns spanned multiple virus species, a few were dominated by a single species, such as human metapneumovirus or respiratory syncytial virus within the *Pneumoviridae* family (Supplementary Fig. 4). These findings may help explain why some infections are associated with greater neurological complications in one sex than the other.

One of the most striking findings was the complete separation of cortical developmental trajectories by sex. Females are often described as developing precociously relative to males, but our results suggest a different picture: female and male cortices follow distinct developmental programs for virus receptors, not simply shifted timelines. This distinction has important implications for understanding the mechanisms underlying sex-specific neurological outcomes after viral infection.

The majority of sex differences occur before puberty

In our study, most sex differences in receptor expression emerged between birth and approximately 12 years, well before puberty. By contrast, a previous time-series analysis of genome-wide transcription across 14 brain areas reported the highest number of sex-biased genes

during puberty (Shi et al., 2016). That study, however, used broad age bins and a relatively small sample size, which may have obscured more gradual, sex-specific patterns emerging earlier in postnatal childhood. While the early sex differences uncovered in our study may be unique to the subset of viral receptor genes analyzed, our results underscore the importance of lifespan study designs for detecting developmental sex differences in the brain, especially those that emerge or fade at specific ages.

The large sex differences in childhood underscore the need for high-quality sex-disaggregated data about the neurological impact of viral infection in children. They also highlight the importance of exploring more targeted, sex-specific treatment strategies for pediatric viral infections. Moreover, the presence of these sex differences during a period of rapid development and refinement of neural circuits raises questions about the long-term impact of viral infections. For example, inflammation caused by viral infections in the developing brain increases the risk for cerebral palsy, autism, schizophrenia, multiple sclerosis, and Parkinson's disease (Hagberg et al., 2012; al-Haddad et al., 2019). The sex differences identified in our study provide a starting point to address the sex-specific impact of molecular mechanisms used by viruses to cause inflammation in the developing brain. Furthermore, those molecular differences may contribute to the prevalence of certain post-infection disorders observed in older children, teens, and adults.

Model systems to study sex differences in the impact of viruses on the brain

Animal models and brain organoids are essential tools for studying viral pathogenesis and host responses. For SARS-CoV-2, hACE2 transgenic mouse models and non-human primates have demonstrated viral neuroinvasion and age-related neuronal damage (Muñoz-Fontela et al.,

2020; Beckman et al., 2022; Martínez-Mármol et al., 2023). Organoid studies have similarly revealed the neuroinvasive potential of SARS-CoV-2, Zika, and Dengue viruses (Abreu et al., 2018; Pellegrini et al., 2020; Song et al., 2021).

However, the over-representation of male animals is a significant shortcoming in understanding the mechanisms contributing to sex-specific symptoms and outcomes of viral infection. Nevertheless, when animal studies are designed to examine the impact of sex on viral infections, key differences are often uncovered (Yirrell et al., 1987; Barna et al., 1996; Wynne et al., 2011; Snyder-Keller et al., 2019; Yan et al., 2021). An ideal animal model should incorporate sex as a biological variable while also capturing a range of host–virus interactions (e.g., age, brain area), thereby improving the translational potential of preclinical studies.

Conclusions

This study highlights the complex spatiotemporal landscape of sex-specific development of ssRNA virus receptors in the human brain. Most sex differences emerged before puberty, were most pronounced in the cortex, and varied across virus families, with the *Pneumoviridae* family showing the strongest dimorphism. Contrary to the idea of females simply "maturing earlier," our findings show that females and males follow distinct developmental programs.

Virus receptors represent the first line of host–pathogen interaction, and their developmental timing and sex-specific expression are likely to influence neurological outcomes. Understanding these patterns could guide the development of more effective, sex-sensitive treatments. Finally, because many neuroinvasive viruses disproportionately affect populations in low-resource settings, these findings underscore the urgent need for sex- and age-disaggregated data in future studies to better mitigate the global impact of viral infections.

Declarations

Ethics approval and consent to participate

The Hamilton Integrated Research Ethics Board approved the study (HiREB #2605) and consent for tissue collection was obtained by the brain banks.

Availability of data and material

The processed dataset analyzed in the current study, along with the R code and supplementary materials (figures and tables), are available on the Open Science Framework (Monteiro et al., 2025).

The original data set is from Kang et. al., (2011) and is available on the Gene Omnibus: (GSE25219).

Competing interests

The authors declare that the research was conducted in the absence of any commercial or financial relationships that could be construed as a competing interest.

Funding

NSERC Grant RGPIN-2020-06403 awarded to KM, NSERC CGS-M awarded to LM and NH, OGS awarded to MP. The funders had no role in study design, data collection and analysis, decision to publish, or manuscript preparation.

Author's contributions

LM Conceptualization, Data curation, Formal analysis, Methodology, Software, Validation, Visualization, Writing – review & editing; NH Conceptualization, Formal analysis, Methodology, Software, Visualization, Writing – original draft,; JL Formal analysis, Software,

Supervision, Visualization, Writing – review & editing; MP Software, Validation, Writing – review & editing; NB Validation, Writing – review & editing; KM Conceptualization, Funding acquisition, Investigation, Methodology, Project administration, Resources, Supervision, Writing – original draft, Writing – review & editing.

Acknowledgements

We recognize that our McMaster University laboratory is located on the traditional territories of the Mississauga and Haudenosaunee nations and within the lands protected by the "Dish with One Spoon" wampum agreement. We thank Rachel Kwan, Brendan Kumagai, Ewalina Jeyanesan, Luke Bai and Adam Gee for help with coding.

References

Abreu, C. M., Gama, L., Krasemann, S., Chesnut, M., Odwin-Dacosta, S., Hogberg, H. T., et al. (2018). Microglia Increase Inflammatory Responses in iPSC-Derived Human BrainSpheres. *Front Microbiol* 9, 2766. doi: 10.3389/fmicb.2018.02766

al-Haddad, B. J. S., Oler, E., Armistead, B., Elsayed, N. A., Weinberger, D. R., Bernier, R., et al. (2019). The fetal origins of mental illness. *Am. J. Obstet. Gynecol.* 221, 549–562. doi: 10.1016/j.ajog.2019.06.013

Alt, H., and Godau, M. (1995). Computing the Fréchet distance between two polygonal curves. *Int. J. Comput. Geom. Appl.* 05, 75–91. doi: 10.1142/s0218195995000064

Barna, M., Komatsu, T., Bi, Z., and Reiss, C. S. (1996). Sex differences in susceptibility to viral infection of the central nervous system. *J. Neuroimmunol.* 67, 31–39. doi: 10.1016/0165-5728(96)00022-7

Beckman, D., Bonillas, A., Diniz, G. B., Ott, S., Roh, J. W., Elizaldi, S. R., et al. (2022). SARS-CoV-2 infects neurons and induces neuroinflammation in a non-human primate model of COVID-19. *Cell Rep.* 41, 111573. doi: 10.1016/j.celrep.2022.111573

Bohmwald, K., Gálvez, N. M. S., Ríos, M., and Kalergis, A. M. (2018). Neurologic Alterations Due to Respiratory Virus Infections. *Front. Cell. Neurosci.* 12, 386. doi: 10.3389/fncel.2018.00386

Calin-Jageman, R. J., and Cumming, G. (2019). Estimation for Better Inference in Neuroscience. *eNeuro* 6, ENEURO.0205-19.2019. doi: 10.1523/eneuro.0205-19.2019

Douaud, G., Lee, S., Alfaro-Almagro, F., Arthofer, C., Wang, C., McCarthy, P., et al. (2022). SARS-CoV-2 is associated with changes in brain structure in UK Biobank. *Nature* 604, 697–707. doi: 10.1038/s41586-022-04569-5

Engin, A. B., Engin, E. D., and Engin, A. (2021). Current opinion in neurological manifestations of SARS-CoV-2 infection. *Curr. Opin. Toxicol.* 25, 49–56. doi: 10.1016/j.cotox.2021.03.004

Hagberg, H., Gressens, P., and Mallard, C. (2012). Inflammation during fetal and neonatal life: Implications for neurologic and neuropsychiatric disease in children and adults. *Ann. Neurol.* 71, 444–457. doi: 10.1002/ana.22620

Ho, J., Tumkaya, T., Aryal, S., Choi, H., and Claridge-Chang, A. (2019). Moving beyond P values: data analysis with estimation graphics. *Nat. Methods* 16, 565–566. doi: 10.1038/s41592-019-0470-3

Jacobsen, H., and Klein, S. L. (2021). Sex Differences in Immunity to Viral Infections. *Front Immunol* 12, 720952. doi: 10.3389/fimmu.2021.720952

Kang, H. J., Kawasawa, Y. I., Cheng, F., Zhu, Y., Xu, X., Li, M., et al. (2011). Spatio-temporal transcriptome of the human brain. Nature 478, 483–489. doi: 10.1038/nature10523

Klein, S. L., and Huber, S. (2009). “Sex Hormones and Immunity to Infection,” in *Sex Differences in Susceptibility to Viral Infection*, eds. S. L. Klein and C. Roberts (Berlin, Heidelberg: Springer), 93–122. doi: 10.1007/978-3-642-02155-8_4

Koyuncu, O. O., Hogue, I. B., and Enquist, L. W. (2013). Virus Infections in the Nervous System. *Cell Host Microbe* 13, 379–393. doi: 10.1016/j.chom.2013.03.010

Kumar, A., Narayan, R. K., Kulandhasamy, M., Prasoon, P., Kumari, C., Kumar, S., et al. (2021). COVID-19 pandemic: insights into molecular mechanisms leading to sex-based differences in patient outcomes. *Expert Rev Mol Med* 23, e7. doi: 10.1017/erm.2021.9

Lehallier, B., Gate, D., Schaum, N., Nanasi, T., Lee, S. E., Yousef, H., et al. (2019). Undulating changes in human plasma proteome profiles across the lifespan. *Nat Med* 25, 1843–1850. doi: 10.1038/s41591-019-0673-2

Lehallier, B., Shokhirev, M. N., Wyss‐Coray, T., and Johnson, A. A. (2020). Data mining of human plasma proteins generates a multitude of highly predictive aging clocks that reflect different aspects of aging. *Aging Cell* 19, e13256. doi: 10.1111/acel.13256

Martínez-Mármol, R., Giordano-Santini, R., Kaulich, E., Cho, A.-N., Przybyla, M., Riyadh, M. A., et al. (2023). SARS-CoV-2 infection and viral fusogens cause neuronal and glial fusion that compromises neuronal activity. *Sci. Adv.* 9. doi: 10.1126/sciadv.adg2248

Mauvais-Jarvis, F., Merz, N. B., Barnes, P. J., Brinton, R. D., Carrero, J.-J., DeMeo, D. L., et al. (2020). Sex and gender: modifiers of health, disease, and medicine. *Lancet* 396, 565–582. doi: 10.1016/s0140-6736(20)31561-0

Mavrikaki, M., Lee, J. D., Solomon, I. H., and Slack, F. J. (2022). Severe COVID-19 is associated with molecular signatures of aging in the human brain. *Nat. Aging* 2, 1130–1137. doi: 10.1038/s43587-022-00321-w

Monteiro, L., Halabian, N., Li, J., Panday, M., Barone, N., and Murphy, K. M. (2025). OSF: Sex- and Age-Specific Development of ssRNA Virus Receptor Expression in the Human Brain. Available at: https://osf.io/4fgka/

Morgello, S. (2020). Coronaviruses and the central nervous system. *J Neurovirol* 26, 1–15. doi: 10.1007/s13365-020-00868-7

Muñoz-Fontela, C., Dowling, W. E., Funnell, S. G. P., Gsell, P.-S., Riveros-Balta, A. X., Albrecht, R. A., et al. (2020). Animal models for COVID-19. Nature 586, 509–515. doi: 10.1038/s41586-020-2787-6

Narayan, A., Berger, B., and Cho, H. (2021). Assessing single-cell transcriptomic variability through density-preserving data visualization. *Nat. Biotechnol.* 39, 765–774. doi: 10.1038/s41587-020-00801-7

Nath, A., and Johnson, T. P. (2022). Mechanisms of viral persistence in the brain and therapeutic approaches. *FEBS J.* 289, 2145–2161. doi: 10.1111/febs.15871

Pellegrini, L., Albecka, A., Mallery, D. L., Kellner, M. J., Paul, D., Carter, A. P., et al. (2020). SARS-CoV-2 Infects the Brain Choroid Plexus and Disrupts the Blood-CSF Barrier in Human Brain Organoids. *Cell Stem Cell* 27, 951-961.e5. doi: 10.1016/j.stem.2020.10.001

Peretz, J., Hall, O. J., and Klein, S. L. (2015). "Sex Differences in Influenza Virus Infection, Vaccination and Therapies," in *Sex and Gender Differences in Infectious Diseases*, eds. S. L. Klein and C. W. Roberts (Springer Cham), 183–210. doi: 10.1007/978-3-319-16438-0

Scully, E. P., Haverfield, J., Ursin, R. L., Tannenbaum, C., and Klein, S. L. (2020). Considering how biological sex impacts immune responses and COVID-19 outcomes. *Nat. Rev. Immunol.* 20, 442–447. doi: 10.1038/s41577-020-0348-8

Shi, L., Zhang, Z., and Su, B. (2016). Sex Biased Gene Expression Profiling of Human Brains at Major Developmental Stages. *Sci Rep-uk* 6, 21181. doi: 10.1038/srep21181

Snyder-Keller, A., Kramer, L. D., Zink, S., and Bolivar, V. J. (2019). Mouse Strain and Sex-Dependent Differences in Long-term Behavioral Abnormalities and Neuropathologies after Developmental Zika Infection. *J. Neurosci.* 39, 5393–5403. doi: 10.1523/jneurosci.2666-18.2019

Song, E., Zhang, C., Israelow, B., Lu-Culligan, A., Prado, A. V., Skriabine, S., et al. (2021). Neuroinvasion of SARS-CoV-2 in human and mouse brain. *J Exp Med* 218, e20202135. doi: 10.1084/jem.20202135

Sudre, C. H., Murray, B., Varsavsky, T., Graham, M. S., Penfold, R. S., Bowyer, R. C., et al. (2021). Attributes and predictors of long COVID. *Nat. Med.* 27, 626–631. doi: 10.1038/s41591-021-01292-y

Sun, S.-H., Chen, Q., Gu, H.-J., Yang, G., Wang, Y.-X., Huang, X.-Y., et al. (2020). A Mouse Model of SARS-CoV-2 Infection and Pathogenesis. Cell Host Microbe 28, 124-133.e4. doi: 10.1016/j.chom.2020.05.020

Takahashi, T., Ellingson, M. K., Wong, P., Israelow, B., Lucas, C., Klein, J., et al. (2020). Sex differences in immune responses that underlie COVID-19 disease outcomes. Nature 588, 315–320. doi: 10.1038/s41586-020-2700-3

Wynne, O., Horvat, J. C., Kim, R. Y., Ong, L. K., Smith, R., Hansbro, P. M., et al. (2011). Neonatal respiratory infection and adult re-infection: Effect on glucocorticoid and mineralocorticoid receptors in the hippocampus in BALB/c mice. *Brain, Behav., Immun.* 25, 1214–1222. doi: 10.1016/j.bbi.2011.03.014

Yan, L., Jayaram, M., Chithanathan, K., Zharkovsky, A., and Tian, L. (2021). Sex-Specific Microglial Activation and SARS-CoV-2 Receptor Expression Induced by Chronic Unpredictable Stress. Front. Cell. Neurosci. 15, 750373. doi: 10.3389/fncel.2021.750373

Yirrell, D. L., Blyth, W. A., and Hill, T. J. (1987). The Influence of Androgens on Paralysis in Mice Following Intravenous Inoculation of Herpes Simplex Virus. *J. Gen. Virol.* 68, 2461–2464. doi: 10.1099/0022-1317-68-9-2461

Zhang, Z., Zhu, Z., Chen, W., Cai, Z., Xu, B., Tan, Z., et al. (2019). Cell membrane proteins with high N-glycosylation, high expression and multiple interaction partners are preferred by mammalian viruses as receptors. *Bioinformatics* 35, 723–728. doi: 10.1093/bioinformatics/bty694

Zhou, F., Yu, T., Du, R., Fan, G., Liu, Y., Liu, Z., et al. (2020). Clinical course and risk factors for mortality of adult inpatients with COVID-19 in Wuhan, China: a retrospective cohort study. *Lancet Lond Engl* 395, 1054–1062. doi: 10.1016/s0140-6736(20)30566-3

Figure Legends

Figure 1. *Workflow for studying sex-specific development of ssRNA virus receptor genes in the brain.* We extracted gene expression data for 67 ssRNA virus receptors from 700 tissue samples (F=306, M=394) across 15 brain areas from the Kang dataset. Lifespan trajectories were plotted by fitting locally estimated scatterplot smoothing (LOESS) curves for each sex for all genes and brain areas. The trajectories were analyzed using high-dimensional data tools, including unsupervised clustering and tSNE visualization, to identify sex-specific developmental patterns. Finally, Differential Sliding Window Analysis (DE-SWAN) was used to identify sex-specific differences in gene expression across the lifespan.

Figure 2. *Lifespan trajectories of ACE2 expression in the female and male brain.* This figure shows the lifespan trajectories for Angiotensin-Converting Enzyme 2 (ACE2) across 15 brain areas in females and males. Z-scored expression values are plotted against age on a logarithmic scale. LOESS curves are fitted for each sex, with shaded bands indicating the 95% confidence interval. Curves are coloured by sex, with red representing females and blue representing males. Brain area abbreviations: A1C: primary auditory cortex, AMY: amygdala, CBC: cerebellar cortex, DFC: dorsolateral prefrontal cortex, HIP: hippocampus, IPC: posterior inferior parietal cortex, ITC: inferior temporal cortex, M1C: primary motor cortex, MFC: medial prefrontal cortex, OFC: orbital prefrontal cortex, S1C: primary somatosensory cortex, STC: superior

temporal cortex, V1C: primary visual cortex, VFC: ventrolateral prefrontal cortex, MD: mediodorsal nucleus of the thalamus.

Figure 3. *Hierarchical clustering of lifespan trajectories across 67 virus receptor genes in the brain.* A) Unsupervised hierarchical clustering (ward.D2 method) of the 2010 lifespan trajectories (67 virus receptor genes × 15 brain areas × 2 sexes) identified 25 distinct clusters. B) For each cluster, all individual trajectories and the cluster-average trajectory are shown. Clusters are labeled based on the proportion of female and male trajectories they contain (e.g., F100:M0, F4:M96).

Figure 4. *Sex differences across gene/brain area trajectory clusters.* A) Sex Bias Index (SBI) for each of the 25 clusters. Positive values (red) indicate a higher proportion of female trajectories, while negative values (blue) indicate a higher proportion of male trajectories in a cluster. B) Examples of the local maxima analysis (black dots) on the average trajectories for the two most female and male-dominated clusters. C) Frequency histogram of the local maxima by age for the 2010 lifespan trajectories. Clusters are ordered as in Figure 3.

Figure 5. *Venn diagrams of female and male trajectories in each of the 25 clusters.* Each Venn diagram shows the proportion of female and male trajectories within a cluster. Overlap indicates that both the female and male trajectories for a gene from the same brain area are included in the cluster. Clusters are ordered as in Figure 3.

Figure 6. *Cluster composition by brain areas.* Pie charts show the percentage of trajectories from each of the 15 brain areas within the 25 clusters. Colours correspond to the anatomical progression of brain areas, with warm colours representing more rostral (e.g., OFC) and cool colours for more caudal regions (e.g., CBC). Clusters are ordered as in Figure 3.

Figure 7. *Cluster composition by virus family.* Pie charts show the percentage of trajectories from each of the 10 virus families within the 25 clusters. Clusters are ordered as in Figure 3.

Figure 8. *Sex bias indices for each virus family and the overall sexual dimorphism score.* (A-J) Sex bias indices (SBI) for the clusters within each of the 10 virus families. Positive values (red) indicate more female trajectories and negative values (blue) more male trajectories in a cluster. (K) Sexual dimorphism score (DS) for each of the 10 virus families. The score can vary from 0, where every cluster has an equal number of female and male trajectories, to 1, where all clusters have either only female or male trajectories.

Figure 9. *Differential Expression Sliding Window Analysis (DE-SWAN) across the 15 brain areas.* DE-SWAN heatmaps show the ages at which females (magenta) or males (green) have higher expression of a virus receptor gene. Each row in the heatmaps represents one of the 67 virus receptor genes, and columns correspond to reference ages. Rows are ordered by a surrounding dendrogram to group similar patterns of gene expression.

Figure 10. *High-dimensional visualization of virus receptor development patterns in the 15 brain areas for females and males.* Density-preserving tSNE plots represent the high-dimensional developmental patterns of all 67 virus receptor genes across both sexes and 15 brain areas. Plots are coloured by A) cluster assignment from brain area-sex hierarchical clustering (k=4), B) age (lighter colours representing younger ages and progressively darker shades representing older ages), and C) sex (female: reddish; male: blueish) and cortical (saturated colours) vs subcortical (unsaturated colours) areas.

Supplementary Figure Legends

Supplementary Figure 1. *Lifespan trajectories.* Locally Estimated Scatterplot Smoothing (LOESS) curves plotted for all 67 genes across all 15 brain areas studied. Z-scored expression values are plotted against age on a logarithmic scale. Shaded bands indicate the 95% confidence interval, and curves are coloured by sex.

Supplementary Figure 2. *Assessing cluster similarity.* Fréchet distance metrics were calculated between each of the 25 developmental trajectory clusters to quantify similarity in trajectory shape and a set of examples are presented here. (A-D) Between-cluster estimation statistics swarm plots showing both the expression values and the distribution of unpaired median differences for each cluster. The left-most cluster in each plot serves as the reference, with all other clusters compared against it. A Fréchet distance distribution greater than 0 indicates that the compared cluster has a trajectory that is different from the reference. A) Swarm plot comparing four clusters to the reference cluster F83:M17. All comparisons show distributions greater than 0, indicating distinct trajectories. B) Swarm plot comparing four clusters to the reference F63:M37. All compared clusters had distributions greater than 0, indicating different trajectories. C) Swarm plot comparing all 25 clusters to the reference F13:M87. All the clusters had trajectories that were different from F13:M87, with distributions greater than 0. D) Swarm

plot comparing all 25 clusters to the reference F81:M19. All the clusters had distributions greater than 0, indicating different trajectories.

Supplementary Figure 3. *Assessing robustness of DE-SWAN.* The number of significantly differentially expressed genes was quantified across age under different analysis parameters. **A)** Varying uncorrected p-value thresholds. **B)** Using q-values after Benjamini–Hochberg false discovery rate (FDR) correction. **C)** Varying sliding window sizes to assess robustness. Inflection points from these plots were used to define the window centers.

Supplementary Figure 4. *Clustering profiles for each virus family.* A) Hierarchical clustering dendrogram of gene expression trajectories associated with each virus family. Clustering was performed independently for each family. B) Average expression trajectories for each cluster within each virus family, ordered by decreasing percent female dominance. C) Venn diagrams representing the percent female dominance for each cluster. D) Pie charts show the distribution of brain areas represented within each cluster. Colour gradient from warm to cool reflects anatomical progression from rostral (OFC) to caudal (CBC) brain areas. E) Pie charts showing the composition of virus species within each cluster. F) Heatmaps showing the proportions of trajectories for each virus receptor gene within each cluster. Rows represent genes, columns represent clusters. Shades of yellow indicate increasing representation, and navy indicates absence of that gene's trajectory within the cluster. Heatmaps are ordered by decreasing percent female dominance.

Supplementary Tables

Supplementary Table 1. *Case Information from Kang dataset.* Table of the cases from the Kang Dataset across 15 brain areas.

Supplementary Table 2. *Virus Receptor Gene List information.* List of viral receptor genes used in this study. Includes names, short forms, and gene symbols with associated viral species.

Supplementary Table 3. *Members of the 25 developmental trajectory clusters.* Table listing the developmental trajectories within each of the 25 clusters, as determined by hierarchical clustering of the 2,010 lifespan trajectories (67 virus receptor genes × 15 brain areas × 2 sexes)

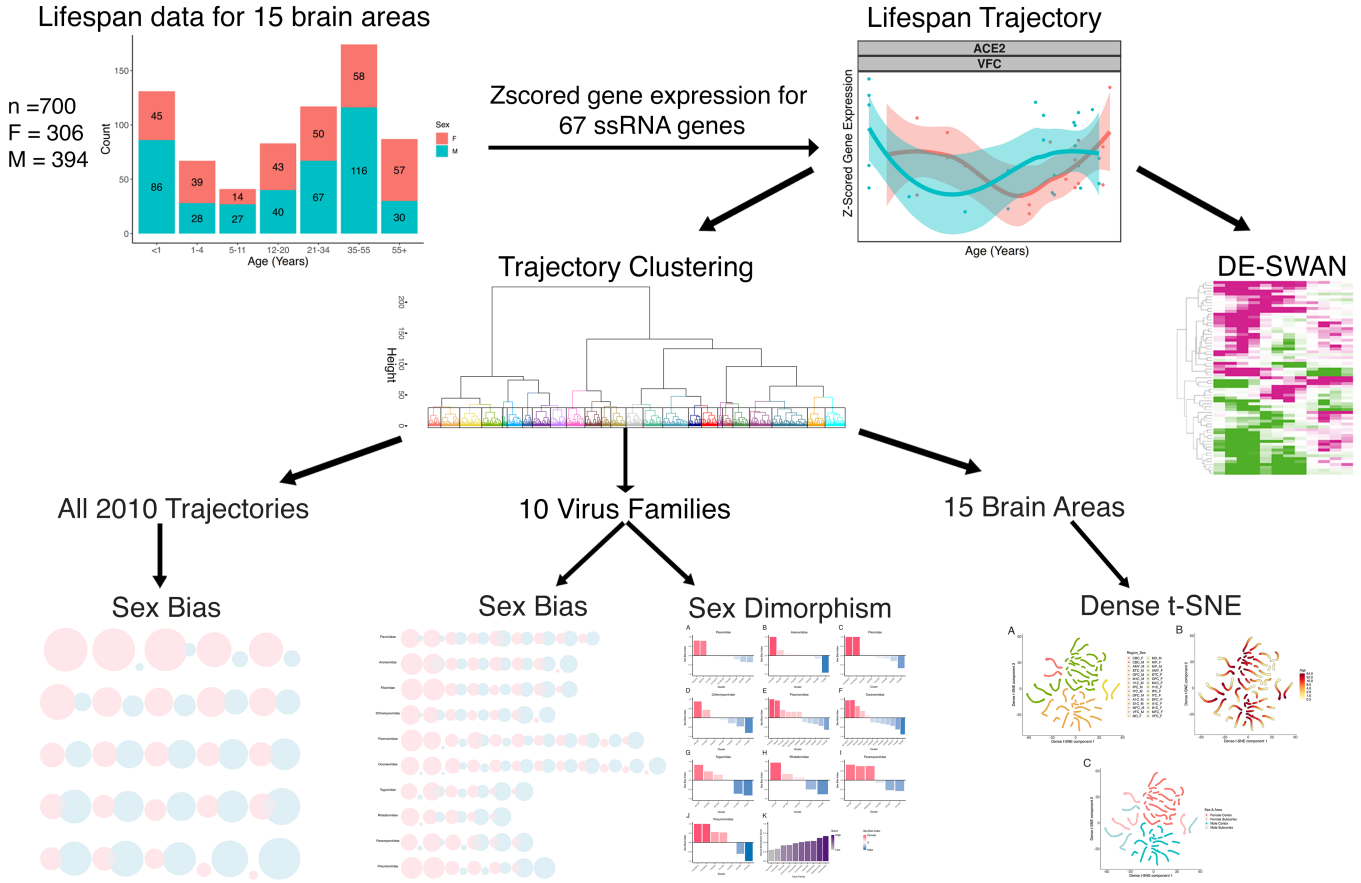
Lifespan data for 15 brain areas
n =700
F = 306
M = 394
Count
Age (Years)
Sex
F
M
Zscored gene expression for
67 ssRNA genes
Lifespan Trajectory
ACE2
VFC
Z-Scored Gene Expression
Age (Years)
Trajectory Clustering
Height
DE-SWAN
All 2010 Trajectories
10 Virus Families
15 Brain Areas
Sex Bias
Sex Bias
Sex Dimorphism
Dense t-SNE

Coronaviridae; Human coronavirus NL63, SARS coronavirus, Severe acute respiratory syndrome coronavirus 2 **ACE2** (Receptor)

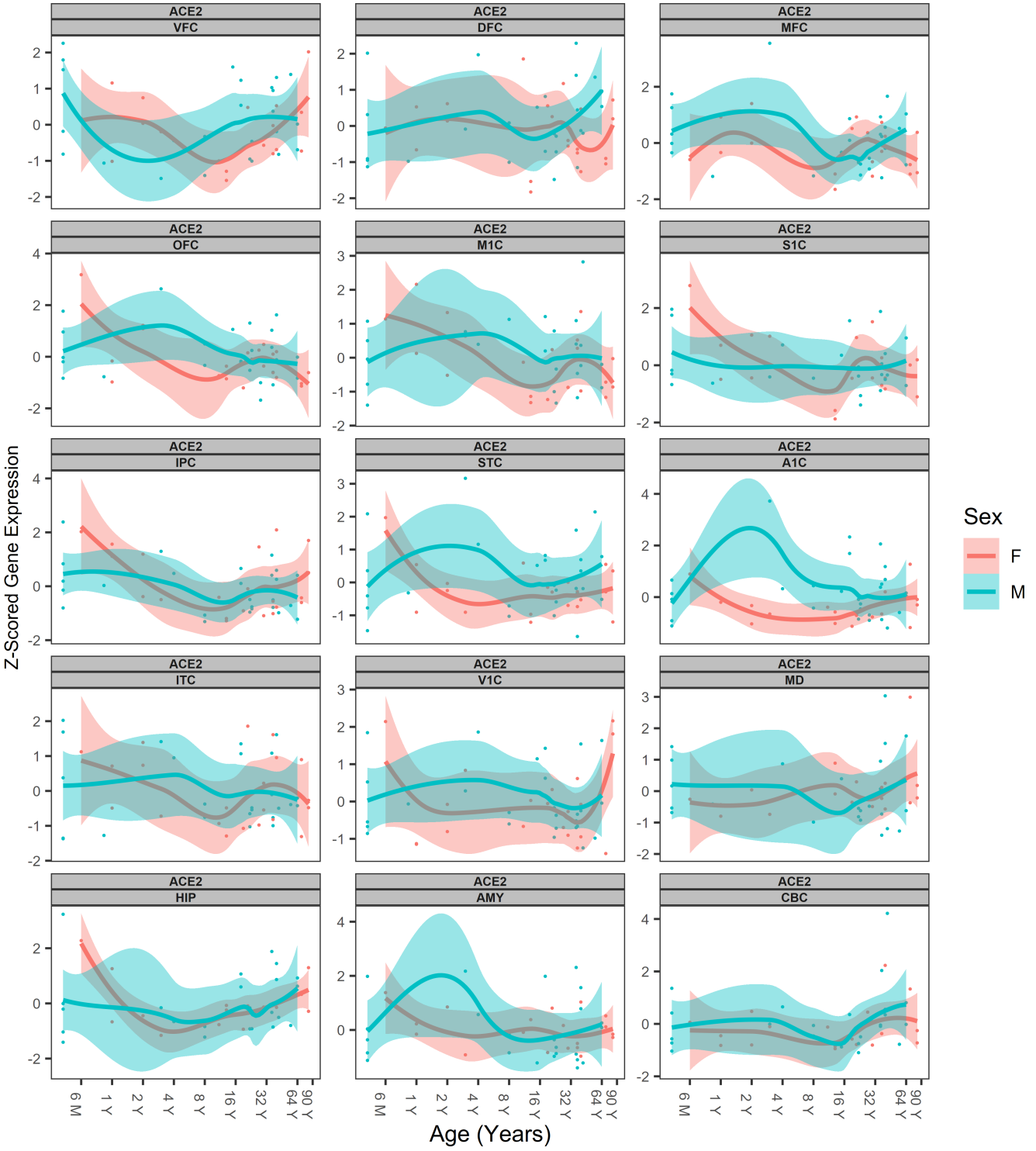

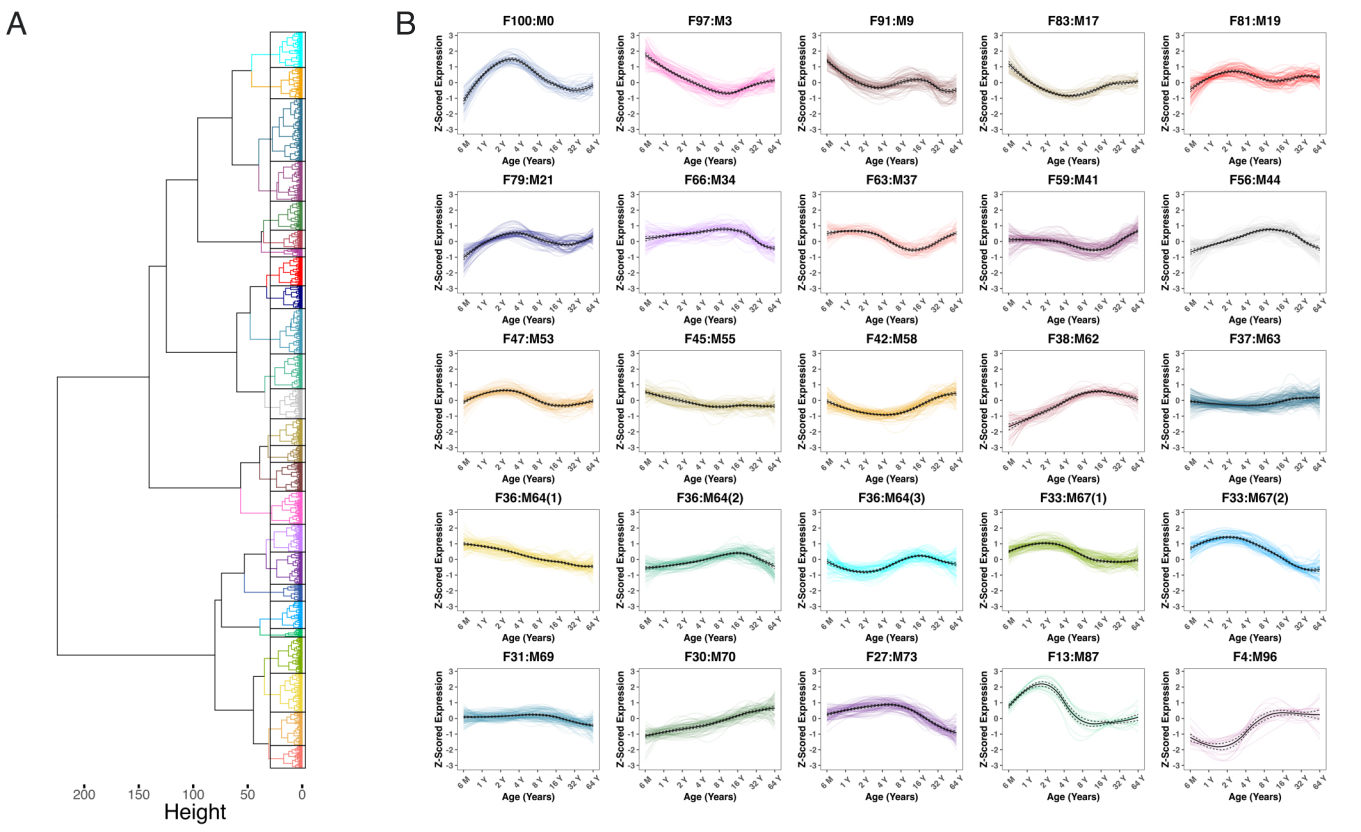
A
200
150
100
50
0
Height
B
F100:M0
F97:M3
F91:M9
F83:M17
F81:M19
F79:M21
F66:M34
F63:M37
F59:M41
F56:M44
F47:M53
F45:M55
F42:M58
F38:M62
F37:M63
F36:M64(1)
F36:M64(2)
F36:M64(3)
F33:M67(1)
F33:M67(2)
F31:M69
F30:M70
F27:M73
F13:M87
F4:M96
Z-Scored Expression
Age (Years)
6 M
1 Y
2 Y
4 Y
8 Y
16 Y
32 Y
64 Y

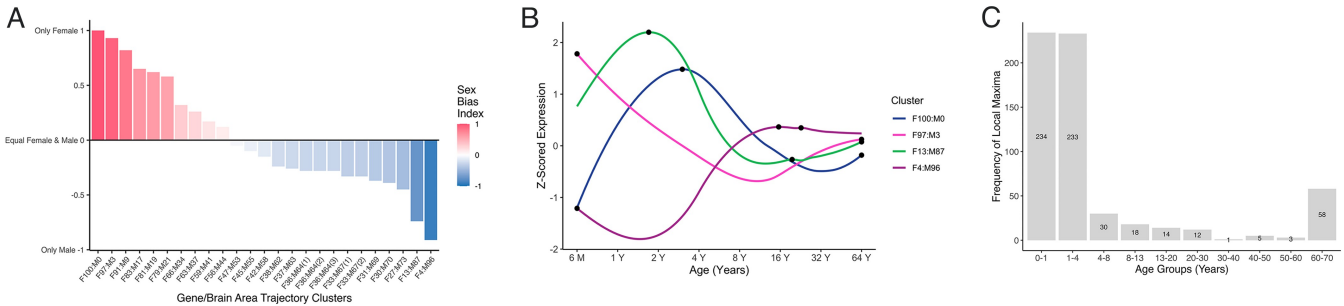
A
Only Female 1
0.5
Equal Female & Male 0
-0.5
Only Male -1
Sex Bias Index
1
0
-1
F100:M0
F97:M3
F91:M9
F83:M17
F81:M10
F79:M21
F66:M34
F63:M37
F59:M41
F58:M44
F47:M53
F45:M55
F42:M58
F38:M62
F37:M63
F36:M64(1)
F36:M64(2)
F36:M64(3)
F33:M67(1)
F33:M67(2)
F31:M69
F30:M70
F27:M73
F13:M87
F4:M96
Gene/Brain Area Trajectory Clusters
B
Z-Scored Expression
2
1
0
-1
-2
6 M
1 Y
2 Y
4 Y
8 Y
16 Y
32 Y
64 Y
Age (Years)
Cluster
F100:M0
F97:M3
F13:M87
F4:M96
C
Frequency of Local Maxima
200
150
100
50
0
234
233
30
18
14
12
1
5
3
58
0-1
1-4
4-8
8-13
13-20
20-30
30-40
40-50
50-60
60-70
Age Groups (Years)

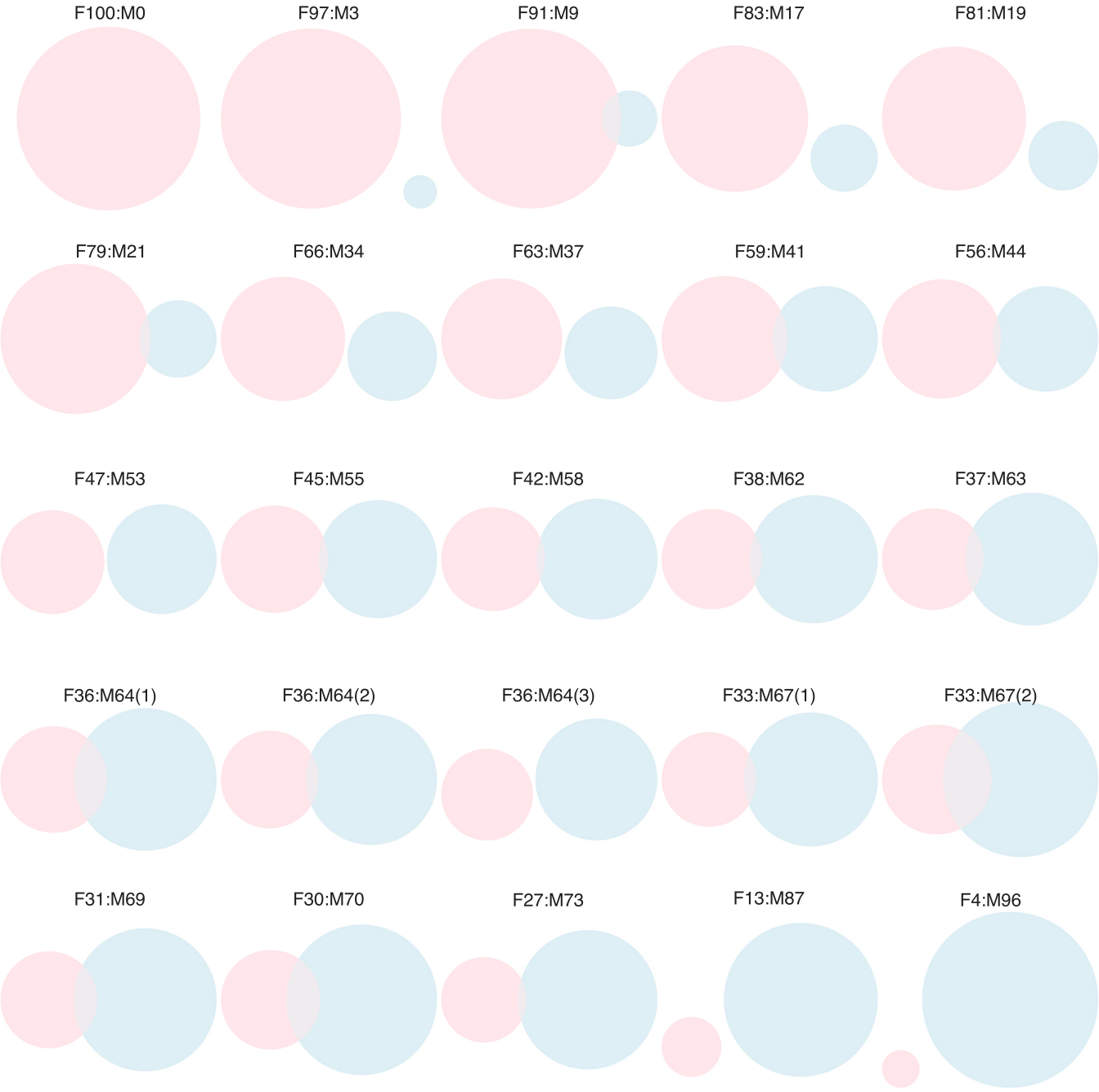
F100:M0
F97:M3
F91:M9
F83:M17
F81:M19
F79:M21
F66:M34
F63:M37
F59:M41
F56:M44
F47:M53
F45:M55
F42:M58
F38:M62
F37:M63
F36:M64(1)
F36:M64(2)
F36:M64(3)
F33:M67(1)
F33:M67(2)
F31:M69
F30:M70
F27:M73
F13:M87
F4:M96

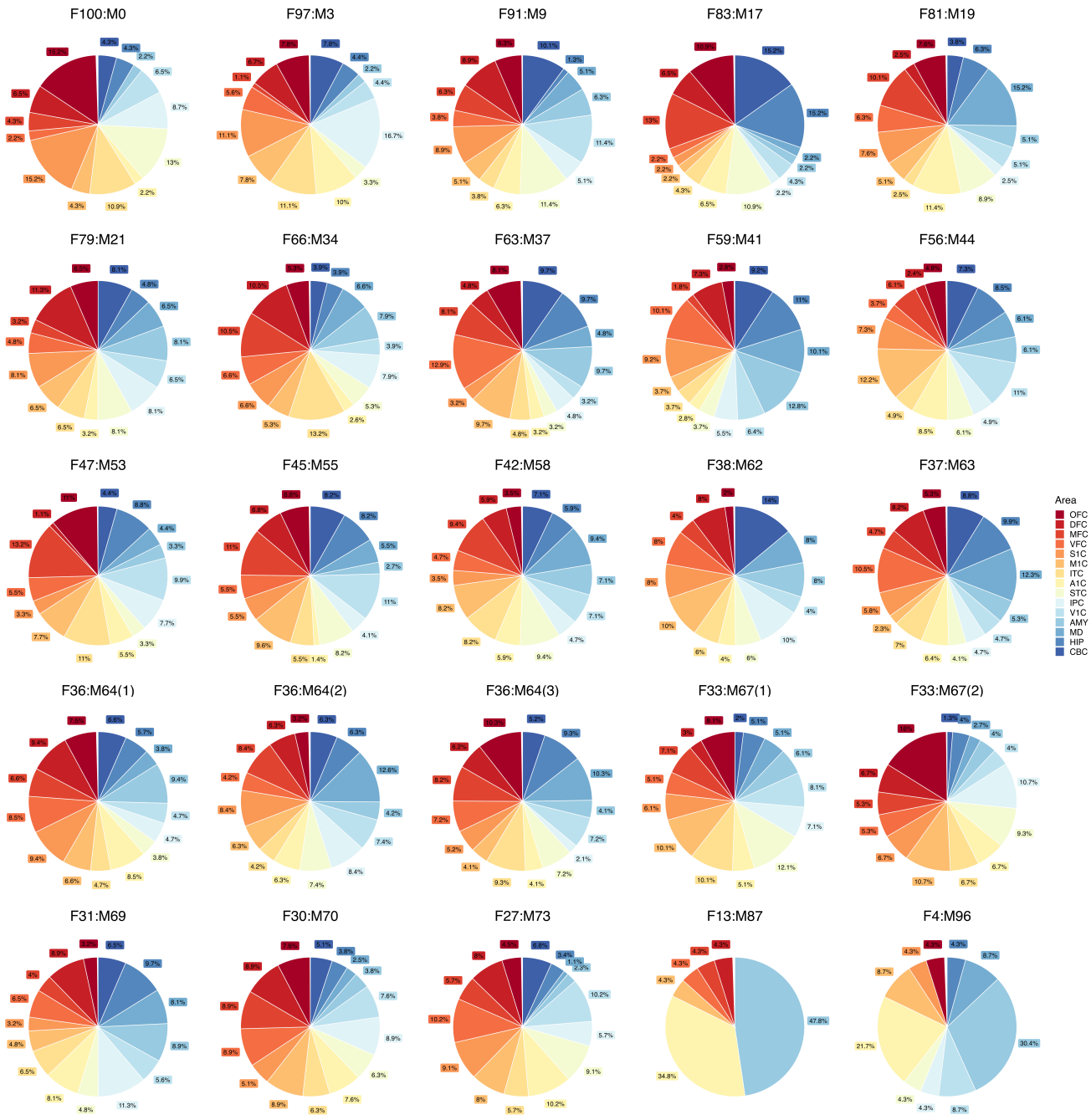
F100:M0
F97:M3
F91:M9
F83:M17
F81:M19
F79:M21
F66:M34
F63:M37
F59:M41
F56:M44
F47:M53
F45:M55
F42:M58
F38:M62
F37:M63
F36:M64(1)
F36:M64(2)
F36:M64(3)
F33:M67(1)
F33:M67(2)
F31:M69
F30:M70
F27:M73
F13:M87
F4:M96
Area
OFC
DFC
MFC
VFC
S1C
M1C
ITC
A1C
STC
IPC
V1C
AMY
MD
HIP
CBC

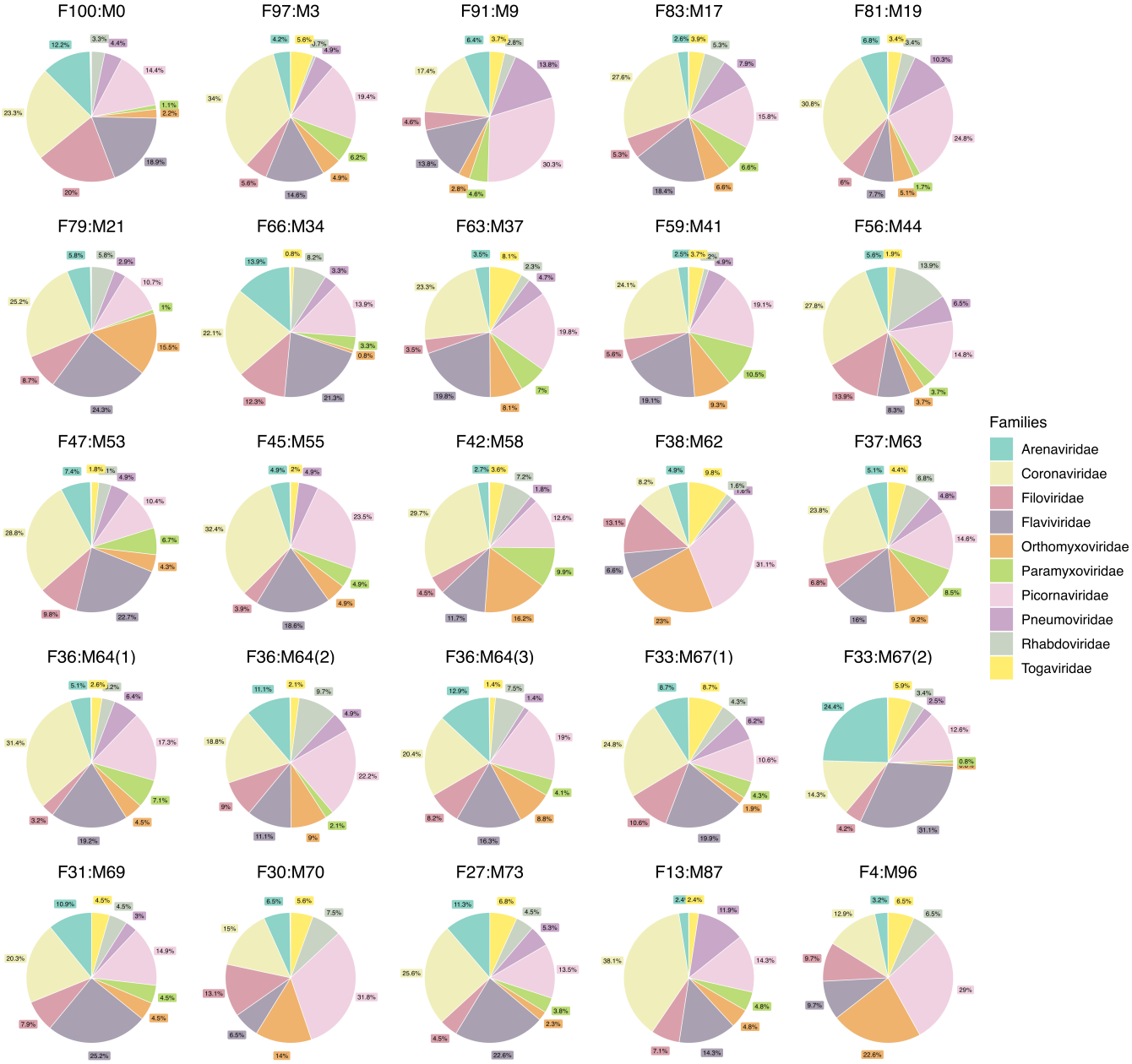
F100:M0
12.2%
3.3%
4.4%
14.4%
1.1%
2.2%
18.9%
20%
23.3%
F97:M3
4.2%
5.6%
1.7%
4.9%
19.4%
6.2%
4.9%
14.6%
5.6%
34%
F91:M9
6.4%
3.7%
2.8%
13.8%
30.3%
4.6%
2.8%
13.8%
4.6%
17.4%
F83:M17
2.6%
3.9%
5.3%
7.9%
15.8%
6.6%
6.6%
18.4%
5.3%
27.6%
F81:M19
6.8%
3.4%
3.4%
10.3%
24.8%
1.7%
5.1%
7.7%
6%
30.8%
F79:M21
5.8%
5.8%
2.9%
10.7%
1%
15.5%
24.3%
8.7%
25.2%
F66:M34
0.8%
8.2%
3.3%
13.9%
3.3%
0.8%
21.3%
12.3%
22.1%
13.9%
F63:M37
3.5%
8.1%
2.3%
4.7%
19.8%
7%
8.1%
19.8%
3.5%
23.3%
F59:M41
2.5%
3.7%
2%
4.9%
19.1%
10.5%
9.3%
19.1%
5.6%
24.1%
F56:M44
5.6%
1.9%
13.9%
6.5%
14.8%
3.7%
3.7%
8.3%
13.9%
27.8%
F47:M53
7.4%
1.8%
1%
4.9%
10.4%
6.7%
4.3%
22.7%
9.8%
28.8%
F45:M55
4.9%
2%
4.9%
23.5%
4.9%
4.9%
18.6%
3.9%
32.4%
F42:M58
2.7%
3.6%
7.2%
1.8%
12.6%
9.9%
16.2%
11.7%
4.5%
29.7%
F38:M62
4.9%
9.8%
1.6%
1.6%
31.1%
23%
6.6%
13.1%
8.2%
F37:M63
5.1%
4.4%
6.8%
4.8%
14.6%
8.5%
9.2%
16%
6.8%
23.8%
F36:M64(1)
5.1%
2.6%
1.2%
8.4%
17.3%
7.1%
4.5%
19.2%
3.2%
31.4%
F36:M64(2)
11.1%
2.1%
9.7%
4.9%
22.2%
2.1%
9%
11.1%
9%
18.8%
F36:M64(3)
12.9%
1.4%
7.5%
1.4%
19%
4.1%
8.8%
16.3%
8.2%
20.4%
F33:M67(1)
8.7%
8.7%
4.3%
6.2%
10.6%
4.3%
1.9%
19.9%
10.6%
24.8%
F33:M67(2)
5.9%
3.4%
2.5%
12.6%
0.8%
31.1%
4.2%
14.3%
24.4%
F31:M69
10.9%
4.5%
4.5%
3%
14.9%
4.5%
4.5%
25.2%
7.9%
20.3%
F30:M70
6.5%
5.6%
7.5%
31.8%
14%
6.5%
13.1%
15%
F27:M73
11.3%
6.8%
4.5%
5.3%
13.5%
3.8%
2.3%
22.6%
4.5%
25.6%
F13:M87
2.4%
2.4%
11.9%
14.3%
4.8%
4.8%
14.3%
7.1%
38.1%
F4:M96
3.2%
6.5%
6.5%
29%
22.6%
9.7%
9.7%
12.9%
Families
Arenaviridae
Coronaviridae
Filoviridae
Flaviviridae
Orthomyxoviridae
Paramyxoviridae
Picornaviridae
Pneumoviridae
Rhabdoviridae
Togaviridae

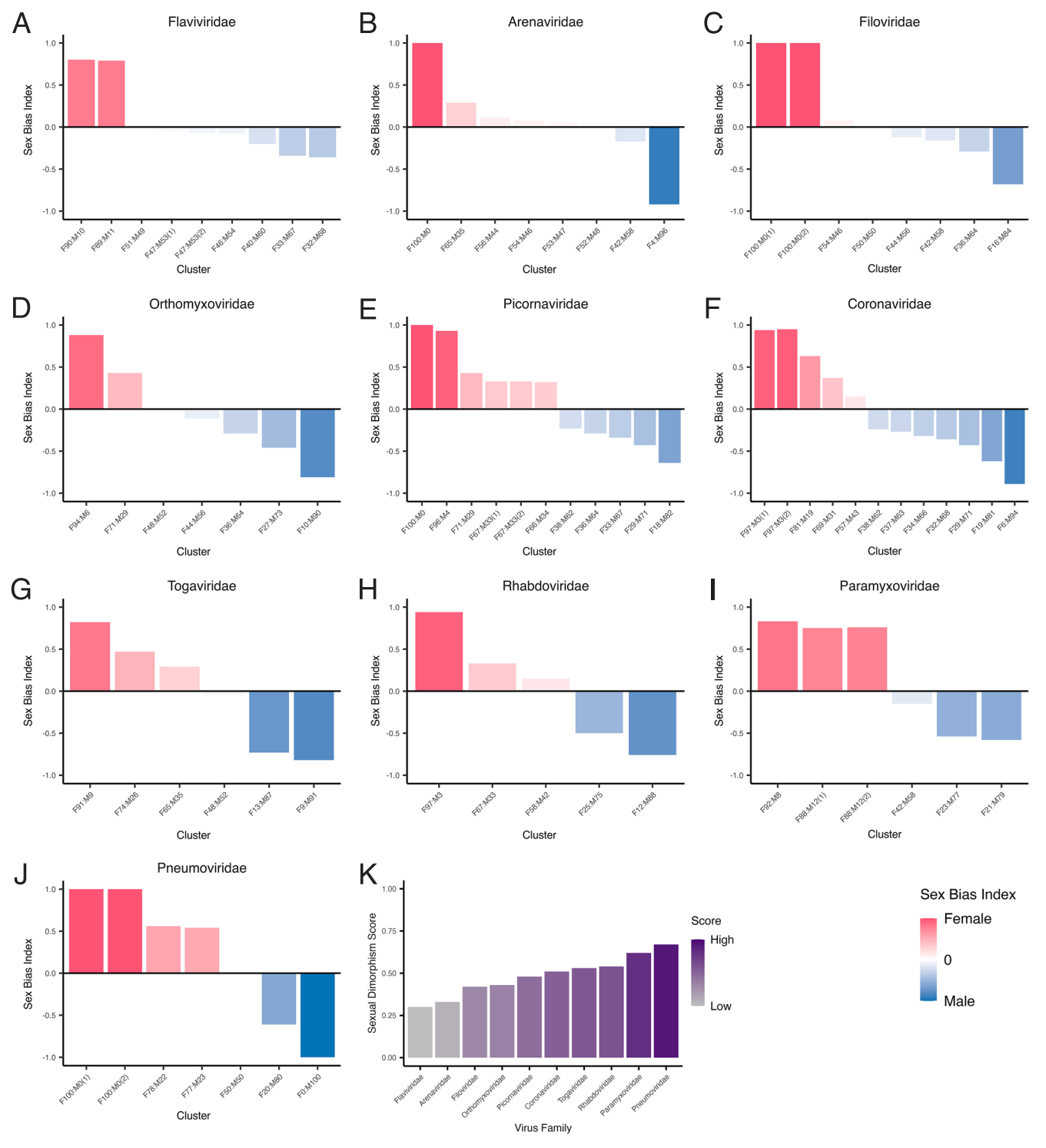
A
Flaviviridae
Sex Bias Index
1.0
0.5
0.0
-0.5
-1.0
F90:M10
F69:M11
F51:M49
F47:M53(1)
F47:M53(2)
F46:M54
F40:M60
F33:M67
F32:M68
Cluster
B
Arenaviridae
Sex Bias Index
F100:M0
F65:M35
F56:M44
F54:M46
F53:M47
F52:M48
F42:M58
F4:M96
Cluster
C
Filoviridae
Sex Bias Index
F100:M0(1)
F100:M0(2)
F54:M46
F50:M50
F44:M56
F42:M58
F36:M64
F16:M84
Cluster
D
Orthomyxoviridae
Sex Bias Index
F94:M6
F71:M29
F48:M52
F44:M56
F36:M64
F27:M73
F10:M90
Cluster
E
Picornaviridae
Sex Bias Index
F100:M0
F96:M4
F71:M29
F67:M33(1)
F67:M33(2)
F66:M34
F38:M62
F36:M64
F33:M67
F29:M71
F18:M82
Cluster
F
Coronaviridae
Sex Bias Index
F97:M3(1)
F97:M3(2)
F81:M19
F69:M31
F57:M43
F38:M62
F37:M63
F34:M66
F32:M68
F29:M71
F19:M81
F6:M94
Cluster
G
Togaviridae
Sex Bias Index
F91:M9
F74:M26
F65:M35
F48:M52
F13:M87
F9:M91
Cluster
H
Rhabdoviridae
Sex Bias Index
F97:M3
F67:M33
F58:M42
F25:M75
F12:M88
Cluster
I
Paramyxoviridae
Sex Bias Index
F92:M8
F88:M12(1)
F88:M12(2)
F42:M58
F23:M77
F21:M79
Cluster
J
Pneumoviridae
Sex Bias Index
F100:M0(1)
F100:M0(2)
F78:M22
F77:M23
F50:M50
F20:M80
F0:M100
Cluster
K
Sexual Dimorphism Score
1.00
0.75
0.50
0.25
0.00
Flaviviridae
Arenaviridae
Filoviridae
Orthomyxoviridae
Picornaviridae
Coronaviridae
Togaviridae
Rhabdoviridae
Paramyxoviridae
Pneumoviridae
Virus Family
Score
High
Low
Sex Bias Index
Female
0
Male

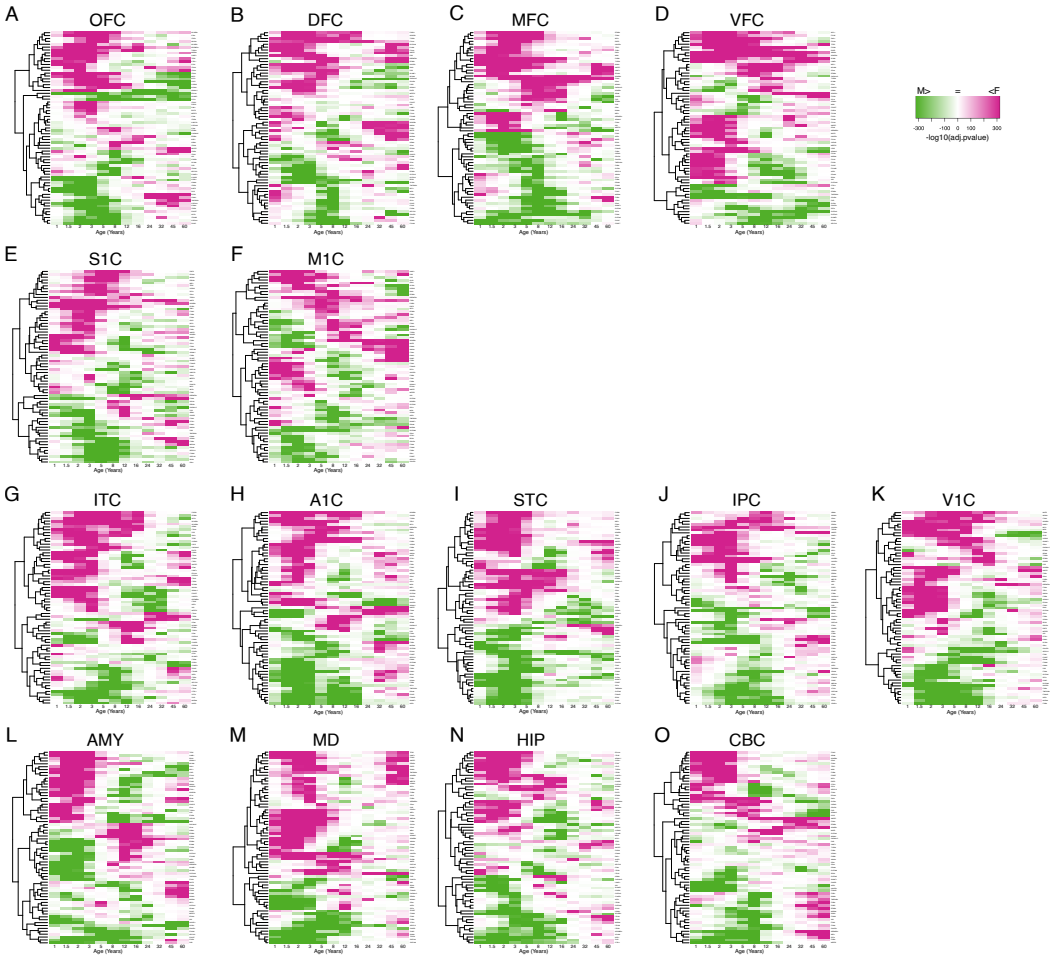
A
OFC
B
DFC
C
MFC
D
VFC
M>
=
<F
-300
-100
0
100
300
-log10(adj.pvalue)
E
S1C
F
M1C
G
ITC
H
A1C
I
STC
J
IPC
K
V1C
L
AMY
M
MD
N
HIP
O
CBC
Age (Years)

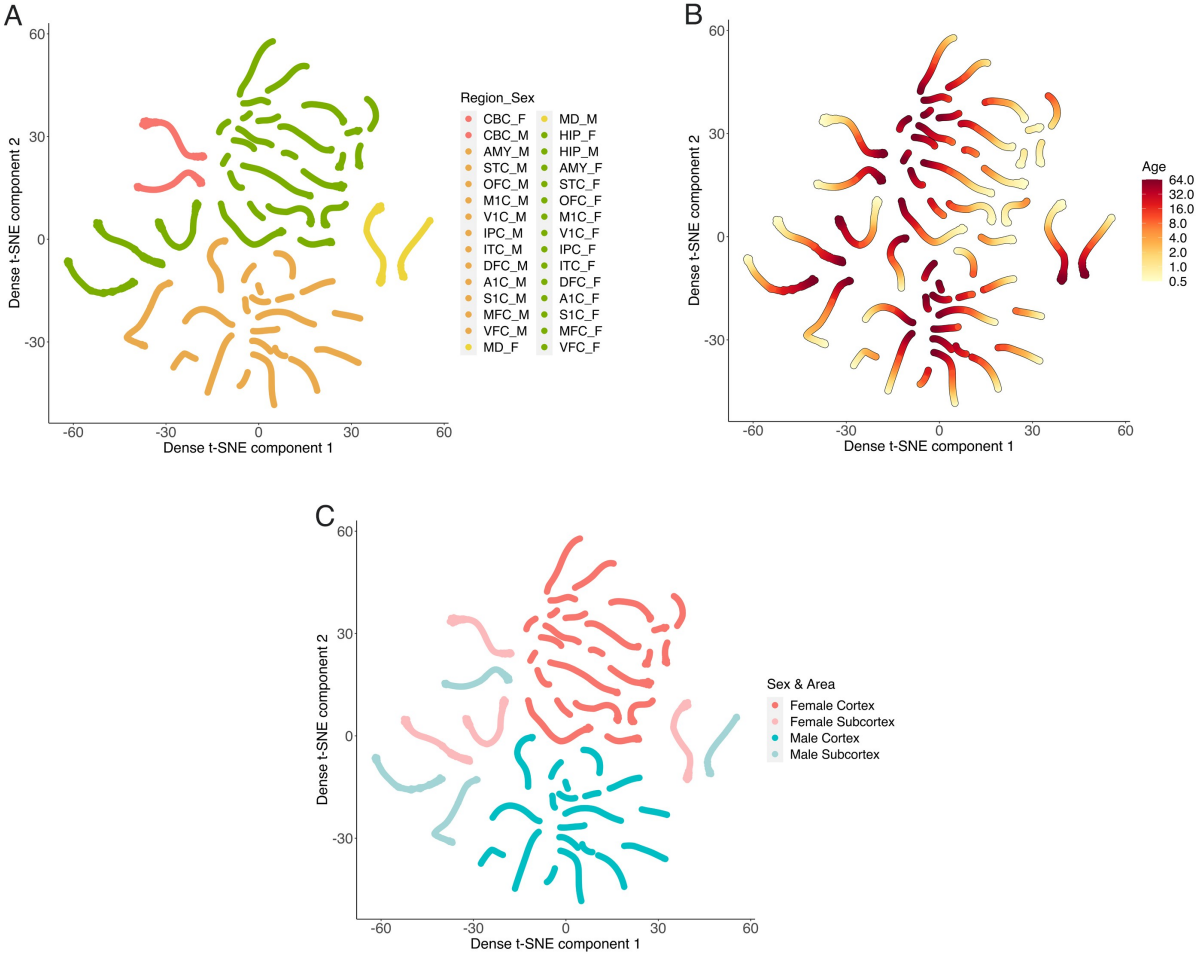
A
Dense t-SNE component 2
Dense t-SNE component 1
60
30
0
-30
-60
-30
0
30
60
Region_Sex
CBC_F
CBC_M
AMY_M
STC_M
OFC_M
M1C_M
V1C_M
IPC_M
ITC_M
DFC_M
A1C_M
S1C_M
MFC_M
VFC_M
MD_F
MD_M
HIP_F
HIP_M
AMY_F
STC_F
OFC_F
M1C_F
V1C_F
IPC_F
ITC_F
DFC_F
A1C_F
S1C_F
MFC_F
VFC_F
B
Dense t-SNE component 2
Dense t-SNE component 1
Age
64.0
32.0
16.0
8.0
4.0
2.0
1.0
0.5
C
Dense t-SNE component 2
Dense t-SNE component 1
Sex & Area
Female Cortex
Female Subcortex
Male Cortex
Male Subcortex